



# Enhancing photoactivity for hydrogen generation by electron tunneling via flip-flop hopping over iodinated graphitic carbon nitride

Zhen Li<sup>a,b</sup>, Bin Tian<sup>a,b</sup>, Wenyuan Zhang<sup>a</sup>, Xuqiang Zhang<sup>a</sup>, Yuqi Wu<sup>a</sup>, Gongxuan Lu<sup>a,\*</sup>

<sup>a</sup> State Key Laboratory for Oxo Synthesis and Selective Oxidation Lanzhou Institute of Chemical Physics, Chinese Academy of Science, Lanzhou 730000, China

<sup>b</sup> University of Chinese Academy of Science, Beijing 100049, China



## ARTICLE INFO

### Article history:

Received 9 September 2016

Received in revised form 8 November 2016

Accepted 10 November 2016

Available online 11 November 2016

### Keywords:

Iodine-decorated graphitic carbon nitride

Flip-flop electron tunneling

Enhanced conductivity

Lifetime of photogenerated charges

High photocatalytic activity for hydrogen generation

## ABSTRACT

In this work, the significant electron tunneling over iodine-decorated graphitic carbon nitride ( $I-g-C_3N_4$ ) was achieved by  $I_3^-$  and  $I_5^-$  clusters implanted. The flip-flop electron tunneling takes place via strong Rashba spin-orbit coupling in p orbitals of polyiodides. The electron tunneling and hopping bridged the easier transfer route between far-located carbon atoms of  $g-C_3N_4$  through the polyiodides p orbitals. By taking the advantage of this tunneling, the conductivity of  $I-g-C_3N_4/Ag$  photocatalyst was remarkably increased and the lifetime of photogenerated charges was largely prolonged, evidenced by I–V characteristics and the photoluminescence (PL) spectra. With the help of these properties, the obtained  $I-g-C_3N_4/Ag$  photocatalyst presented high active for hydrogen generation under visible light irradiation and Ag NPs as active site for hydrogen formation.  $104.3 \mu\text{mol H}_2$  was evolved over  $I-g-C_3N_4/Ag$  photocatalyst in 3 h, about three time higher than that of un-iodinated  $g-C_3N_4/Ag$ , and no remarkable decay of activity was observed in 900 min reaction. The highest AQE value of 7.3% was achieved at 520 nm.

© 2016 Elsevier B.V. All rights reserved.

## 1. Introduction

Photocatalytic water splitting for hydrogen generation driven by sunlight irradiation is one of the most promising routes to store the solar energy [1–6]. Photocatalytic hydrogen evolution system usually contains a metal-based cocatalyst, a photosensitizer and a sacrificial electron donor [7]. In order to achieve high efficiency of hydrogen generation, many efforts have been done in searching excellent electron conductive material to improve the charge separation efficiency [8], broadening the photo response range [9] and utilizing highly active cocatalysts [10]. Among them, improving the charge separation efficiency is a critical factor to obtain an excellent hydrogen evolution activity.

The rapid electron transfer can enhance the charge separation and decrease carrier recombination probability. This objective required material holding good electrical conductivity to promise high electron transfer rate. Graphene and graphitic carbon nitride materials are potential candidates because they have adjacent carbon atoms with both  $\sigma$  bond and  $\pi$  bond. Although the  $\sigma$  electron is strongly restricted by the atom core, however, the  $\pi$  electron is relatively delocalized. The  $\pi$  bonds can build  $\pi$  ribbons, provid-

ing a tunneling route for the electron transfer [11], leading to better conductivity, and are beneficial for photocatalytic reaction [12–14].

Implanting semiconductor NPs and metal NPs on the surface of graphene [15,16] or graphitic carbon nitride [17,18] is an effective way to improve photocatalytic activity, such as incorporating graphene with Pt NPs [19],  $TiO_2$  [20],  $BiVO_4$  [21], etc., due to efficient charge separation and easier transfer from the conduction band of semiconductors or the exited dye to graphene, leading to a significant enhancement of  $H_2$  evolution activity. Unfortunately, attempts to further improving their lower conductivity and mobility meet difficulties partially because of the effect of residual oxygen functional groups and vacancy defects [22,23]. Further enhancing the electrical conductivity of graphene and graphitic carbon nitride is urgent for achieving higher  $H_2$  evolution activity.

Iodine has been widely applied in improving the electrical conductivity of polymer materials [24–26]. It is known that graphene and graphitic carbon nitride has a similar conjugate structure to conducting polymers. Density functional calculations and topological simulations confirmed that charge transfer occurred between iodine and the nanotube wall in the case of linear triiodide ( $I_3^-$ ) and pentaiodide ( $I_5^-$ ) intercalated molecules [27]. In addition, first-principle density-functional calculations revealed that graphene edges could provide decent adsorption sites for halogen atom combination [28]. In fact, many attempts had been devoted to improve the electrical conductivity of carbon materials by doping iodine

\* Corresponding author.

E-mail address: [gxl@lzb.ac.cn](mailto:gxl@lzb.ac.cn) (G. Lu).

species in fuel cells research. For example, Kalita et al. confirmed that iodine doping of graphene can enhance the electron transfer between atomic iodine and graphene surface by the aid of polyiodides ( $I_3^-$  and  $I_5^-$ ) species [29,30]. Zhan et al. found the iodinated graphene exhibited higher reversible capacity, longer-term stability and more excellent performance at very high current density. With doping  $I_3^-$ , the positive charge density on the graphene was increased, leading to excellent electrochemical activity [31]. It was already confirmed that the  $I_3^-$  and  $I_5^-$  interacted with carbon atoms through a charge transfer process could reduce the resistance of carbon materials and improve the electron transfer rate [32,33]. However, less works have been devoted to understand the mechanism of charge transfer iodinated  $g\text{-}C_3\text{N}_4$ . For example, Wang et al. found that iodine existing in the lattice of conjugated polymers could increase their electrical conductivity [34]. Our recent work found that the exceptional electrical properties of  $I_3^-$  and  $I_5^-$  cluster decorated carbon materials might attribute to a larger Rashba spin-orbit coupling induced by heavy adatoms with active electrons living in p orbitals [35]. The tunneling opened by the polyiodides p orbitals could lead an electron hopping between two neighbor carbon atoms in graphene, which gave the superior charge transfer performance. Considering the similar property between graphene and graphitic carbon nitride, we deduce the  $I_3^-$  and  $I_5^-$  cluster can also induce an flip-flop electron tunneling bridge between far-located carbon atoms on  $g\text{-}C_3\text{N}_4$  by strong Rashba spin-orbit coupling in p orbitals over polyiodides decorated  $g\text{-}C_3\text{N}_4$ .

In the view of above, we developed a route of fabrication of iodinated  $g\text{-}C_3\text{N}_4$  photocatalyst by in situ AgI NPs decomposition using light irradiation method. The structure and chemical states of iodine species were characterized through XPS and XRD spectroscopy. The results suggested that I species were in the forms of  $I_3^-$  and  $I_5^-$ . I-V curves showed the  $I_3^-$  and  $I_5^-$  decorated  $g\text{-}C_3\text{N}_4$  exhibited better electrical conductivity and could enhance electron transfer properties, which remarkably reduced the recombination of electron and hole, and prolonged the lifetime of photogenerated charges. The iodinated  $g\text{-}C_3\text{N}_4$  photocatalyst performed higher activity and long-term stability for hydrogen generation. About  $104.3\text{ }\mu\text{mol H}_2$  was generated over I-g-C<sub>3</sub>N<sub>4</sub>/Ag photocatalyst in 3 h, about three time higher than that of un-iodinated  $g\text{-}C_3\text{N}_4$ /Ag. No remarkable decay of activity was observed during 900 min reaction. The highest AQE value of 7.3% was achieved at 520 nm.

## 2. Experimental

### 2.1. Preparation of the $g\text{-}C_3\text{N}_4$ photocatalyst

Typically, 20 g of urea powder was put into a crucible with a cover and then heated to 550 °C within 30 min in a muffle furnace under the protection of nitrogen and maintained at this temperature for 3 h. The resultant powder was cooled to room temperature, washed with ultrapure water, collected by filtration and finally dried at room temperature.

### 2.2. Photocatalytic $H_2$ evolution activity and AQE measurements

Photocatalytic experiments were performed in a sealed Pyrex flask (150 ml) with a flat window (an efficient irradiation area of 14 cm<sup>2</sup>) and a silicone rubber septum for sampling at ambient temperature. In a typical reaction system, 20 mg  $g\text{-}C_3\text{N}_4$  was added into 100 ml 10% (v/v) TEOA aqueous solution. After 30 min ultrasonic treatment, 1 ml 0.1 M AgNO<sub>3</sub> aqueous solution was added into the suspension drop by drop and then the 1 ml 0.1 M KI aqueous solution was added in the same way. This suspension was stirred for 30 min. Subsequently, 70 mg EY was added into the suspension. Prior to irradiation, the suspension was degassed by bubbling Ar gas

for 30 min. The light source was a 300-W Xe lamp, which equipped with either a 420 nm cut-off filter or various band-pass filters. Photon flux of the incident light was determined using a Ray virtual radiation actinometer (FU 100, silicon ray detector, light spectrum, 400–700 nm; sensitivity,  $10\text{--}50\text{ }\mu\text{V }\mu\text{mol}^{-1}\text{ m}^{-2}\text{ s}^{-1}$ ). The amount of H<sub>2</sub> was measured using gas chromatography (Agilent 6820, TCD, 13 × column, Ar carrier), and the AQE was calculated from the ratio of the number of reacted electrons during oxygen evolution to the number of incident photons by the following equation:

$$\text{AQE}[\%] = 2 \times \text{number of evolved H}_2\text{ molecules} / \text{number of incident photons} \times 100$$

### 2.3. Working electrode preparation and photoelectrochemical measurements

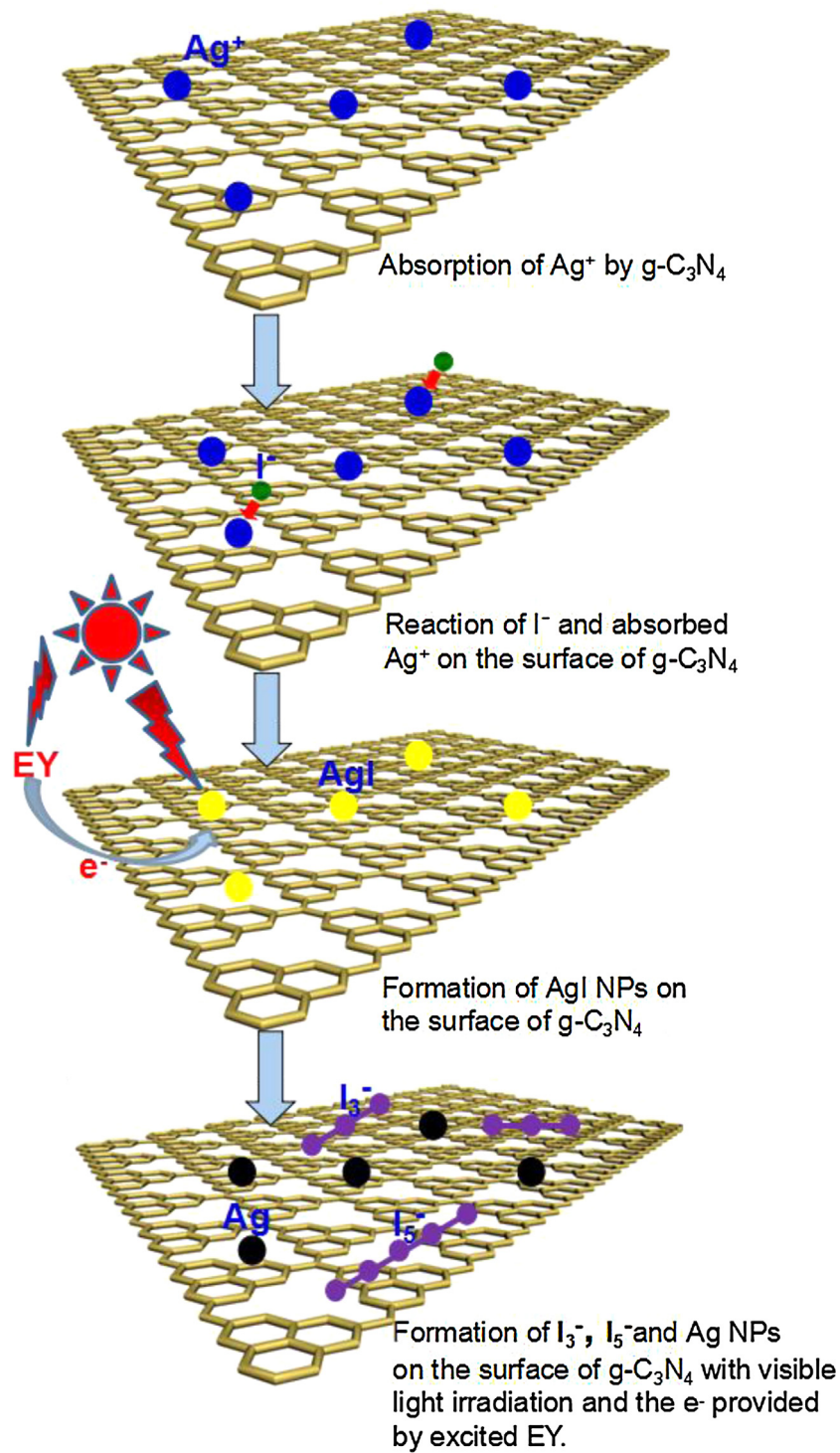
Photocurrent responses of catalyst samples were measured on an electrochemical analyzer (CHI660E) in a homemade standard three-compartment cell, consisting of an organic glass enclosure with a quartz window and a 1.2 cm diameter opening opposite the window to the work electrode was clamped. The working electrodes were prepared by drop-coating sample suspensions directly onto the precleaned indium tin oxide glass (ITO glass) surface by microsyringe with an infrared heat lamp to speed drying. The surface of working electrode exposed to the electrolyte was a circular film with the geometrical surface areas of 1 cm<sup>2</sup>. Platinum foil was used as a counter electrode and a saturated calomel electrode (SCE) was used as the reference electrode. The supporting electrolyte was 10% TEOA aqueous solution mixed with 0.1 M Na<sub>2</sub>SO<sub>4</sub> aqueous solution. A 300-W Xe lamp with an optical cutoff filter ( $\lambda \geq 420\text{ nm}$ ) was used for excitation light source. The unbiased anodic photocurrent was investigated with an amperometric current-time technique.

### 2.4. Characterizations

Transmission electron microscopy (TEM) images were taken with a Tecnai-G2-F30 field emission transmission electron microscope operating at accelerating voltage of 300 kV. The X-ray diffraction patterns (XRD) of the samples were recorded on a Rigaku B/Max-RB X-ray diffractometer with a nickel-filtrated Cu K $\alpha$  radiation. The accelerating voltage and current were 40 kV and 30 mA, respectively. XPS analysis was performed using a VG Scientific ESCALAB210-XPS photoelectron spectrometer with a Mg K $\alpha$ -ray resource. FT-IR spectra were measured on a Nexus 870 FT-IR spectrometer from KBr pellets as the sample matrix. UV-vis Diffuse Reflectance Spectra were obtained with a Shimadzu UV-3600 UV-vis-near-IR spectrophotometer. BaSO<sub>4</sub> was used as a reflectance standard. The fluorescence decay times and PL spectra were measured using the Horiba Jobin Yvon Data Station HUB operating in time-correlated single photon counting mode (TCSPC) with the time resolution of 200 ps. Nano LED diode emitting pulse at 460 nm with 1 MHz repetition rate was used as an excitation source. Light-scattering Ludox solution was used to obtain the instrument response function (prompt). The time ranges are 0.055 ns/channel in 4096 effective channels. Horiba Jobin Yvon DAS6 fluorescence decay analysis software was used to fit the model functions to the experimental data. The I-V curves of the specimens were measured by the 2-probe method on a Keithley 4200 semiconductor characterization system (electrode contact area of  $2.56 \times 10^{-6}\text{ m}^2$ ) at room temperature in air environment.

## 3. Results and discussion

The mechanism of formation of the Ag NPs,  $I_3^-$  and  $I_5^-$  on the surface of  $g\text{-}C_3\text{N}_4$  is illustrated in **Scheme 1**. The  $g\text{-}C_3\text{N}_4$  suspension was dispersed by ultrasound in 10% (v/v) TEOA solution to



**Scheme 1.** The mechanism of the  $\text{Ag}$  NPs,  $\text{I}_3^-$  and  $\text{I}_5^-$  formation on the  $g\text{-C}_3\text{N}_4$  surface.

achieve homogeneous  $g\text{-C}_3\text{N}_4$  dispersion, and then the  $\text{AgNO}_3$  solution was added slowly and drop by drop into the suspension, in which  $\text{Ag}^+$  was first adsorbed on the surface of  $g\text{-C}_3\text{N}_4$  by coulomb forces due to its negative charge. After stirring ten minutes, the  $\text{KI}$  solution was added in the same way, resulting in  $\text{AgI}/g\text{-C}_3\text{N}_4$  composite. Under provided electron by excited EY and the visible light irradiation, the  $\text{AgI}$  NPs were decomposed to form  $\text{Ag}$  NPs,  $\text{I}_3^-$  and  $\text{I}_5^-$  clusters on the surface of  $g\text{-C}_3\text{N}_4$ . In order to prove the decomposition of  $\text{AgI}$  NPs, the XRD characterizations of  $g\text{-C}_3\text{N}_4$ ,  $\text{I-g-C}_3\text{N}_4$ ,  $g\text{-C}_3\text{N}_4/\text{Ag}$  and  $\text{I-g-C}_3\text{N}_4/\text{Ag}$  photocatalysts were carried out

and the result was shown in Fig. 1. For the  $g\text{-C}_3\text{N}_4$  photocatalyst, the strongest diffraction peak at  $27.4^\circ$  ( $d=0.325$ ) was belonged to the dense interlayer-stacking (002) peak of aromatic segment, as a graphite-like packing characteristic of  $g\text{-C}_3\text{N}_4$  materials [36,37]. The peak at  $13.1^\circ$  (0.713 nm) was attributed to (100) peak that arose from the in-plane ordering of tri-s-triazine units [38]. After implanting  $\text{Ag}$  or  $\text{AgI}$  specie on the surface of  $g\text{-C}_3\text{N}_4$ , a series of new peaks centered at  $38.2$ ,  $44.3$ ,  $64.6$ ,  $77.5$ ,  $81.7^\circ$  were detected, which could be assigned to (111), (200), (220), (311) and (222) facets of metal  $\text{Ag}$ , respectively. This result indicates that the  $\text{AgI}$  specie was

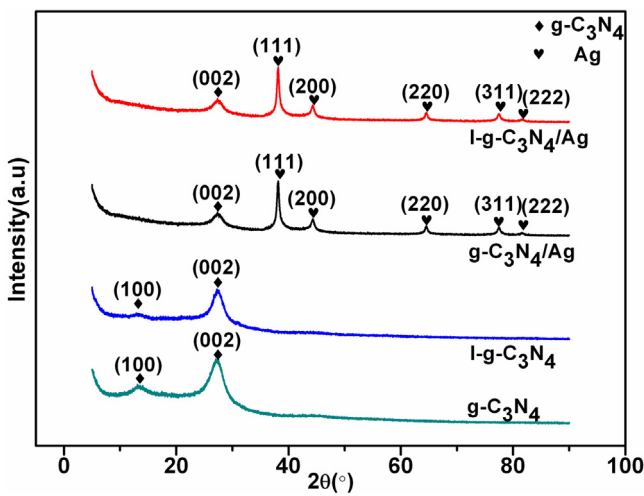


Fig. 1. XRD patterns of  $\text{g-C}_3\text{N}_4$ ,  $\text{I-g-C}_3\text{N}_4$ ,  $\text{g-C}_3\text{N}_4/\text{Ag}$  and  $\text{I-g-C}_3\text{N}_4/\text{Ag}$  photocatalysts.

decomposed in the form of metal Ag on the surface of  $\text{g-C}_3\text{N}_4$ . However, the peak centered at  $13.1^\circ$  was disappeared after loading Ag or  $\text{AgI}$  specie on the surface of  $\text{g-C}_3\text{N}_4$ , implying that a strong inter-

action existed between the Ag NPs and  $\text{g-C}_3\text{N}_4$ . In addition, there were no obvious changes on the peaks of  $\text{g-C}_3\text{N}_4$  and no other peaks were detected when  $\text{I}^-$  was added in the  $\text{g-C}_3\text{N}_4$  dispersion.

To further study the chemical states of Ag and I species, the XPS spectra of  $\text{g-C}_3\text{N}_4$ ,  $\text{I-g-C}_3\text{N}_4$ ,  $\text{g-C}_3\text{N}_4/\text{Ag}$  and  $\text{I-g-C}_3\text{N}_4/\text{Ag}$  photocatalysts were measured and the results were shown in Fig. 2. In Fig. 2A, the peak of C 1s spectra of  $\text{g-C}_3\text{N}_4$  centered at 288.3 eV could be attributed to  $\text{sp}^2$ -bonded carbon ( $\text{N}-\text{C}=\text{N}$ ) species, while the weak one at 286.3 eV could be attributed to  $\text{sp}^3$ -bonded carbon ( $\text{N}-\text{C}$ ) species [39]. After loading  $\text{AgI}$ , Ag and I species on the surface of  $\text{g-C}_3\text{N}_4$ , these binding energy peaks were no obvious shift. In Fig. 2B, the XPS spectra of  $\text{g-C}_3\text{N}_4$  showed that the peak centered at 398.9 eV corresponded to  $\text{sp}^2$  hybridized aromatic N bonded to carbon atoms ( $\text{C}=\text{N}-\text{C}$ ). The peak centered at 399.7 eV corresponded to the tertiary N bonded to carbon atoms in the form of  $\text{N}-(\text{C})_3$  or  $\text{H}-\text{N}-(\text{C})_2$  [40]. The weaker peak with a high binding energy at 401.4 eV corresponded to quaternary N bonded to three carbon atoms in the aromatic cycles [40,41]. And the peak centered at 404.5 eV belonged to the  $\pi$  excitation [42,43]. After loading  $\text{AgI}$ , Ag and I species on the surface of  $\text{g-C}_3\text{N}_4$ , the peaks shifted slightly to low binding energy, corresponding to 398.8, 398.7 and 398.5 eV, respectively. These results also indicated that there were an interaction between Ag, I species and  $\text{g-C}_3\text{N}_4$ , which could promote the electron transfer between  $\text{g-C}_3\text{N}_4$  and Ag NPs. In Fig. 2C, the binding

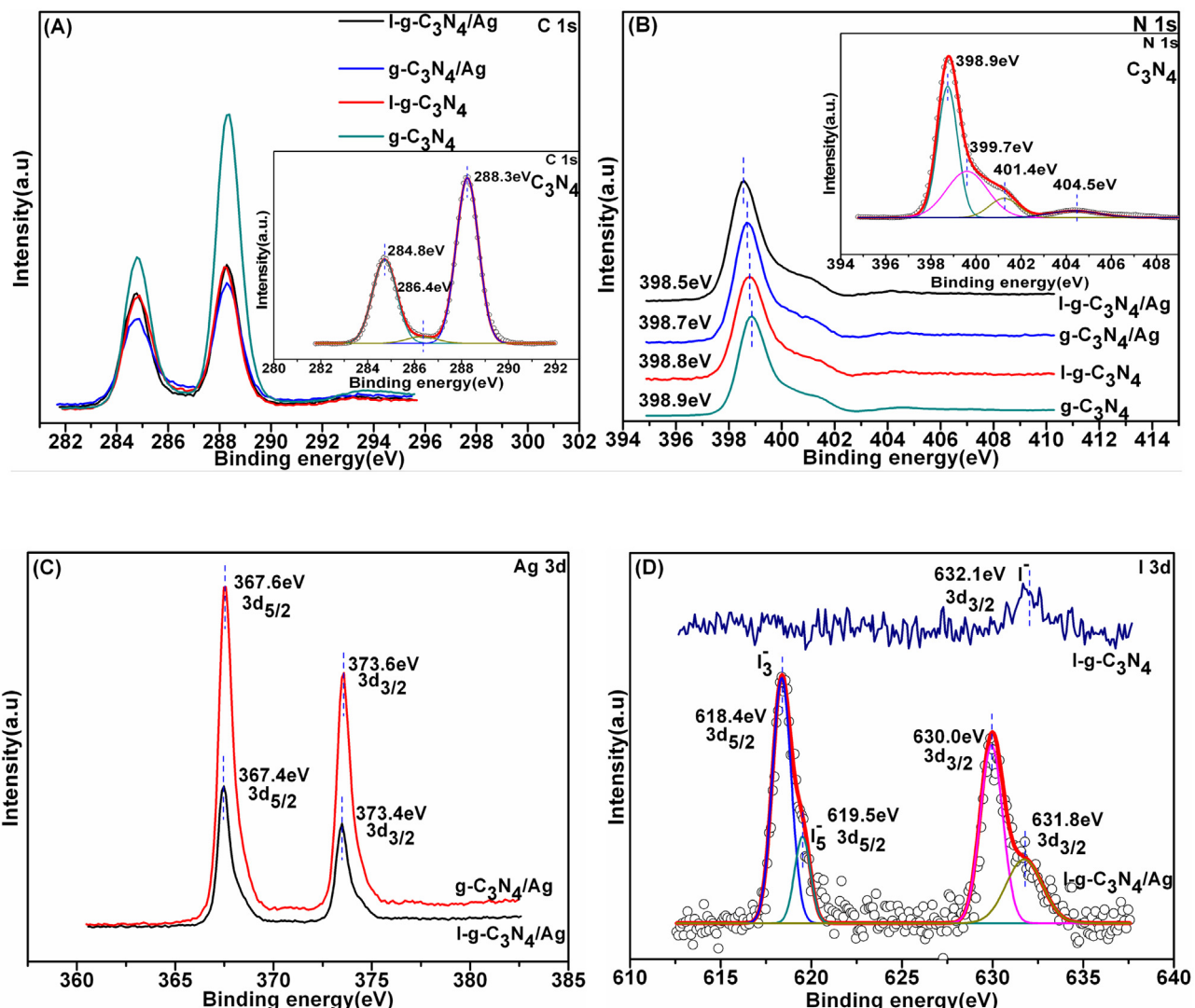


Fig. 2. The XPS spectra of  $\text{g-C}_3\text{N}_4$ ,  $\text{I-g-C}_3\text{N}_4$ ,  $\text{g-C}_3\text{N}_4/\text{Ag}$  and  $\text{I-g-C}_3\text{N}_4/\text{Ag}$  photocatalysts. A) C1s spectra. B) N1s spectra. C) Ag 3d spectra. D) I 3d spectra.

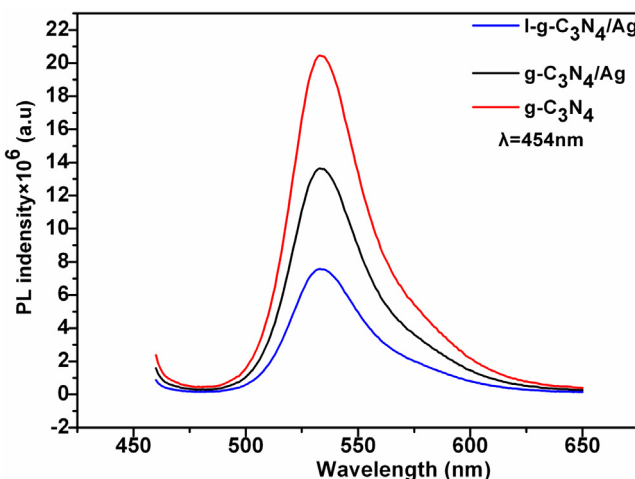


Fig. 3. PL spectra of EY in  $\text{g-C}_3\text{N}_4$ ,  $\text{g-C}_3\text{N}_4/\text{Ag}$  and  $\text{I-g-C}_3\text{N}_4/\text{Ag}$  suspension.

energy of Ag showed that the Ag species were in the metal state and a slight difference was detected between the  $\text{g-C}_3\text{N}_4/\text{Ag}$  and  $\text{I-g-C}_3\text{N}_4/\text{Ag}$  photocatalysts. This result might be resulted by the effect of I species. In Fig. 2D, the peaks centered at 618.4 and 619.5 eV were attributed to  $\text{I}_3^-$  and  $\text{I}_5^- 3\text{d}_{5/2}$ , indicating I specie existed in the form of  $\text{I}_3^-$  and  $\text{I}_5^-$  clusters over the  $\text{I-g-C}_3\text{N}_4/\text{Ag}$  photocatalyst. The  $\text{I}_3^-$  and  $\text{I}_5^-$  clusters could lead to a larger Rashba spin-orbit coupling with active electrons living in p orbitals. The tunneling of an electron between two carbon atoms of  $\text{g-C}_3\text{N}_4$  through the polyiodides p orbitals opens additional channels for hopping, which give rise to the superior charge transfer performance [35]. However, for the  $\text{I-g-C}_3\text{N}_4$  photocatalyst, only a weak peak centered at 632.1 eV was detected, which suggested the I specie existed in the form of  $\text{I}^-$  over  $\text{I-g-C}_3\text{N}_4$  photocatalyst and only a trace amount of  $\text{I}^-$  absorbed on the surface of  $\text{g-C}_3\text{N}_4$ .

The photoluminescence (PL) spectra were carried out to confirm the promotion of the electron transfer rate on the surface of  $\text{g-C}_3\text{N}_4$  by  $\text{I}_3^-$  and  $\text{I}_5^-$  clusters and the result was shown in Fig. 3. The strong PL of EY in  $\text{g-C}_3\text{N}_4$  suspension indicated the fast carrier recombination, and an obvious quenching effect could be observed after loading Ag NPs on the surface of  $\text{g-C}_3\text{N}_4$ , implying that the strong interaction was existed between Ag NPs and  $\text{g-C}_3\text{N}_4$ , which could enhance the electron transfer rate from EY to  $\text{g-C}_3\text{N}_4$  and then from  $\text{g-C}_3\text{N}_4$  to Ag NPs to reduce the recombination of photogenerated charges. However, the quenching effect was further enhanced after the  $\text{I}_3^-$  and  $\text{I}_5^-$  clusters formed on the surface of  $\text{g-C}_3\text{N}_4/\text{Ag}$ . This result suggested the  $\text{I}_3^-$  and  $\text{I}_5^-$  clusters could promote the elec-

tron transfer on the surface of  $\text{g-C}_3\text{N}_4$ , which could further enhance charge separation and prolong of charge lifetime to achieve highly efficient activity of  $\text{H}_2$  evolution. The same conclusion was also identified by the fluorescence lifetime as shown in Table 1. The emission decay of EY in TEOA solution was single-exponential, suggesting that there was only one emitting species (monomeric EY molecules). After addition of  $\text{g-C}_3\text{N}_4$ , the emission decay of EY- $\text{g-C}_3\text{N}_4$  in TEOA solution was two-exponential[44]. The long-lived (1.76 ns) and short-lived (1.28 ns) components were probably resulted from the  $\pi$ -conjugated electronic interaction between EY molecules and  $\text{g-C}_3\text{N}_4$  and the monomeric EY molecules [45]. This result suggests that there was an interaction between EY and  $\text{g-C}_3\text{N}_4$  and the  $\text{g-C}_3\text{N}_4$  could rapidly transfer the electron from excited EY [46]. By loading  $\text{I}^-$  on the surface of  $\text{g-C}_3\text{N}_4$ , the lifetime didn't change obviously, which indicated that the  $\text{I}^-$  was no contribution to prolong the charge lifetime. However, after loading metal Ag NPs on the surface of  $\text{g-C}_3\text{N}_4$ , the average lifetime was increased from 1.36 ns to 2.35 ns, which implied Ag NPs also had an interaction with  $\text{g-C}_3\text{N}_4$ . In this process, the interaction could enhance the electron transfer from  $\text{g-C}_3\text{N}_4$  to Ag NPs. In addition, after the  $\text{I}_3^-$  and  $\text{I}_5^-$  clusters formed on the surface of  $\text{g-C}_3\text{N}_4/\text{Ag}$ , the average lifetime was further prolonged, corresponding to 2.80 ns. This result further proved the  $\text{I}_3^-$  and  $\text{I}_5^-$  clusters could enhance the electron transfer on the surface of  $\text{g-C}_3\text{N}_4$ , which could remarkably reduce the recombination of carrier and prolonged the lifetime of photogenerated charges [10,19]. The I-V electrochemical curves were carried out to further study the effect of the  $\text{I}_3^-$  and  $\text{I}_5^-$  on the electron transfer of the  $\text{g-C}_3\text{N}_4$  and the results were shown in Fig. 4. In Fig. 4A, the  $\text{g-C}_3\text{N}_4$  and  $\text{I-g-C}_3\text{N}_4$  photocatalysts showed typical semiconductor properties. However, after loading Ag NPs on the surface of  $\text{g-C}_3\text{N}_4$ , the  $\text{g-C}_3\text{N}_4/\text{Ag}$  photocatalyst exhibited conductor property. This result indicated that the Ag NPs could improve the electrical conductivity of  $\text{g-C}_3\text{N}_4$  and promote the electron transfer rate. The electrical conductivity of  $\text{g-C}_3\text{N}_4/\text{Ag}$  photocatalyst was further improved with loading  $\text{I}_3^-$  and  $\text{I}_5^-$  clusters on the surface of the  $\text{g-C}_3\text{N}_4$ , suggesting that the  $\text{I}_3^-$  and  $\text{I}_5^-$  clusters could bridge the easier transfer route between far-located carbon atoms of  $\text{g-C}_3\text{N}_4$  enhance to give rise to the excellent conductivity. The tunneling could enhance the electron transfer fast on the surface of  $\text{g-C}_3\text{N}_4$ , leading to remarkably reduce the recombination of carrier and prolonged the lifetime of photogenerated charges.

In order to study the structure and morphology of  $\text{g-C}_3\text{N}_4/\text{Ag}$  and  $\text{I-g-C}_3\text{N}_4/\text{Ag}$  photocatalysts, transmission electron microscopy (TEM) was performed and the results were shown in Fig. 5. The Fig. 5A and B showed that the Ag NPs of  $\text{g-C}_3\text{N}_4/\text{Ag}$  and  $\text{I-g-C}_3\text{N}_4/\text{Ag}$  photocatalysts were distributed uniformly on the surface of  $\text{g-C}_3\text{N}_4$ . The diameters of these Ag NPs were in 6–22 nm. In Fig. 5C, the

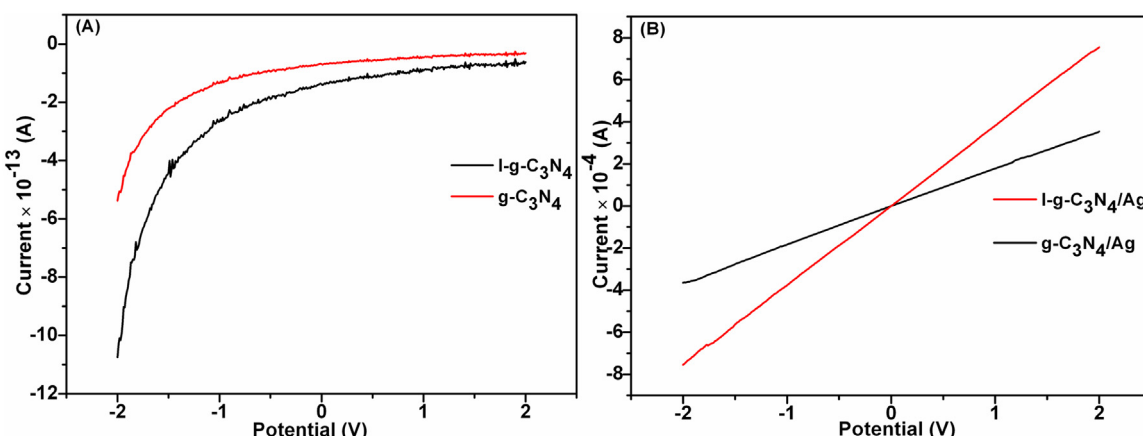


Fig. 4. The I-V electrochemical curves of photocatalysts. ( $1/R = I/U$ ).

**Table 1**Fluorescence lifetime results of EY in g-C<sub>3</sub>N<sub>4</sub>, I-g-C<sub>3</sub>N<sub>4</sub>, g-C<sub>3</sub>N<sub>4</sub>/Ag and I-g-C<sub>3</sub>N<sub>4</sub>/Ag suspension.

C <sub>3</sub> N <sub>4</sub> systems	Lifetime, $\langle \tau \rangle$ (ns)	Pre-exponential factors $B$	Average lifetime, $\langle \tau \rangle$ (ns)	$\chi^2$
EY	$\tau_1 = 1.23$	$B_1 = 1$	1.23	1.0004
EY-g-C <sub>3</sub> N <sub>4</sub>	$\tau_1 = 1.28$ $\tau_2 = 1.76$	$B_1 = 0.8248$ $B_2 = 0.1752$	1.36	0.9967
EY-I-g-C <sub>3</sub> N <sub>4</sub>	$\tau_1 = 1.27$ $\tau_2 = 1.81$	$B_1 = 0.8105$ $B_2 = 0.1895$	1.37	0.9992
EY-g-C <sub>3</sub> N <sub>4</sub> /Ag	$\tau_1 = 1.67$ $\tau_2 = 3.21$	$B_1 = 0.5572$ $B_2 = 0.4428$	2.35	1.0031
EY-I-g-C <sub>3</sub> N <sub>4</sub> /Ag	$\tau_1 = 1.74$ $\tau_2 = 3.52$	$B_1 = 0.4032$ $B_2 = 0.5968$	2.80	1.0009

element composition clearly showed that the distribution of C, N, O and I elements were relatively homogeneous in I-g-C<sub>3</sub>N<sub>4</sub>/Ag photocatalyst. This result indicated the I<sub>3</sub><sup>−</sup> and I<sub>5</sub><sup>−</sup> clusters were distributed uniformly on the surface of g-C<sub>3</sub>N<sub>4</sub>. However, the Ag specie was in the form of cluster. This conclusion was also achieved by the element composition of g-C<sub>3</sub>N<sub>4</sub>/Ag photocatalyst as shown

in Fig. 5D. In Fig. 5E, the I<sup>−</sup> were distributed uniformly on the surface of g-C<sub>3</sub>N<sub>4</sub>.

The time courses of H<sub>2</sub> evolution in 10% (v/v) TEOA aqueous solution under visible light irradiation ( $\lambda \geq 420$  nm) conditions were shown in Fig. 6. No H<sub>2</sub> was evolved over g-C<sub>3</sub>N<sub>4</sub> photocatalyst and only a trace amount of H<sub>2</sub> evolved over I-g-C<sub>3</sub>N<sub>4</sub> photocatalyst,

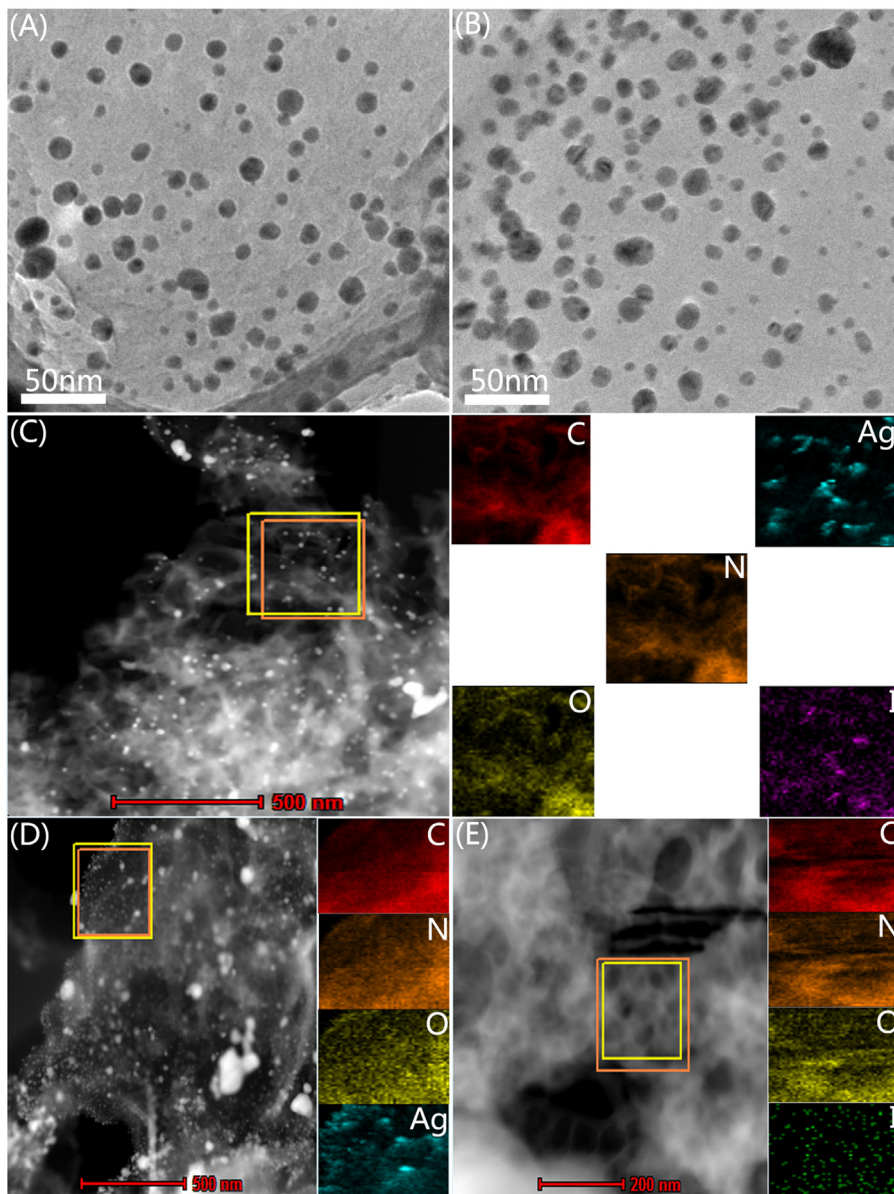


**Fig. 5.** Transmission electron microscopy images of I-g-C<sub>3</sub>N<sub>4</sub>/Ag (A) and g-C<sub>3</sub>N<sub>4</sub>/Ag photocatalyst (B); elemental mapping images of I-g-C<sub>3</sub>N<sub>4</sub>/Ag (C), g-C<sub>3</sub>N<sub>4</sub>/Ag (D) and I-g-C<sub>3</sub>N<sub>4</sub> (E) photocatalysts.

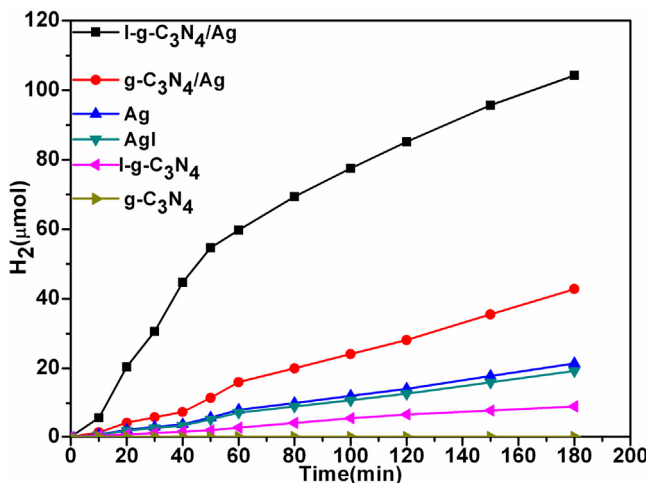


Fig. 6. The time courses of  $H_2$  evolution catalyzed by  $I-g-C_3N_4/Ag$ ,  $g-C_3N_4/Ag$ ,  $I-g-C_3N_4$ ,  $AgI$ ,  $Ag$  and  $g-C_3N_4$  with EY sensitization under visible light irradiation conditions ( $\lambda \geq 420 \text{ nm}$ ) at pH 9.

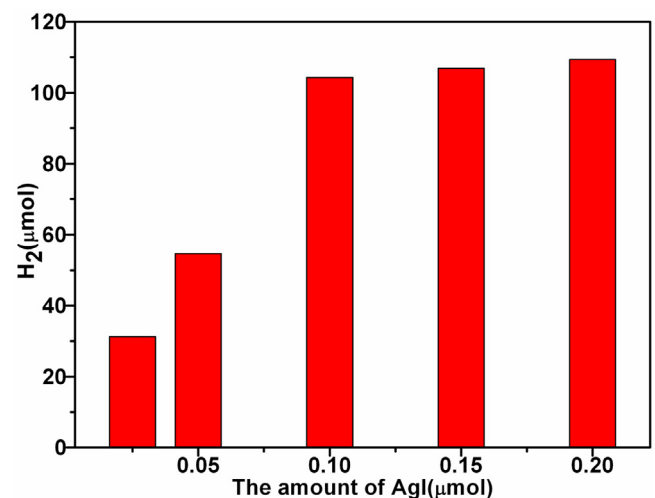


Fig. 8. The effect of the amount of  $AgI$  on the activity of  $H_2$  evolution  $g-C_3N_4$  photocatalyst under visible light irradiation ( $\lambda \geq 420 \text{ nm}$ ).

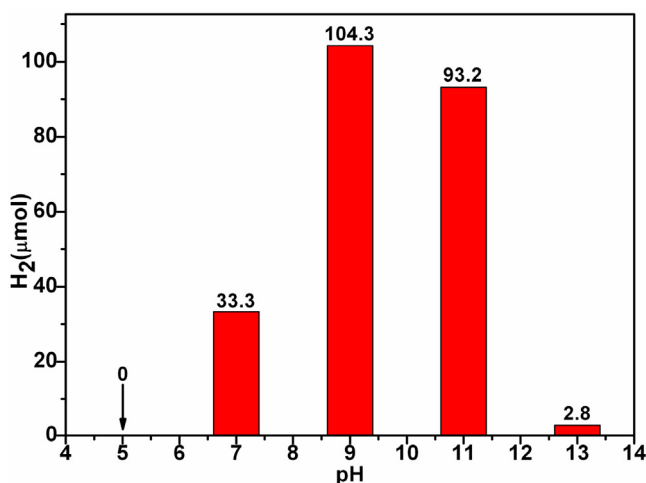


Fig. 7. The effect of pH on photocatalytic activity of  $I-g-C_3N_4/Ag$  photocatalyst with EY sensitization for hydrogen evolution.

implying  $g-C_3N_4$  and  $I-g-C_3N_4$  photocatalysts were inactivity for  $H_2$  evolution. 19.3 and 21.4  $\mu\text{mol}$   $H_2$  evolved over  $AgI$  and  $Ag$  photocatalyst. However, after loading  $Ag$  NPs on the surface of  $g-C_3N_4$ , the rate of  $H_2$  evolution was enhanced (42.8  $\mu\text{mol}$  in 3 h). It might result by confinement effect of  $g-C_3N_4$  for  $Ag$  NPs growth and excellent charge conductivity for  $H_2$  evolution. It also suggested the  $Ag$  was the active site for  $H_2$  evolution. With the  $I_3^-$  and  $I_5^-$  clusters formed on the surface of  $g-C_3N_4$ , the activity of  $H_2$  evolution was further improved significantly on the condition of  $Ag$  as active site, corresponding to 104.3  $\mu\text{mol}$  in 3 h. This result showed that the  $I_3^-$  and  $I_5^-$  clusters could lead to a larger Rashba spin-orbit coupling with active electrons living in p orbitals [35].

The activities of  $H_2$  evolution at different pH (5, 7, 9, 11 and 13) were investigated to optimize the reaction condition and the results were shown in Fig. 7. The highest activity of  $H_2$  evolution was achieved at pH 9. About 104.3  $\mu\text{mol}$  of  $H_2$  was evolved over  $I-g-C_3N_4/Ag$  photocatalyst in EY sensitized suspension dispersion. With the increase of acidity, the activity of  $H_2$  evolution gradually decreased due to the protonation of TEOA in acidic solution [44]. That process of protonation would impact the electron-donating properties of TEOA and the absorption performance of EY in the visible light region. However, with the increase of alkaline, 93.2  $\mu\text{mol}$  of  $H_2$  was generated in 3 h at pH 11. Further increasing the alka-

line, the  $H_2$  evolution rate was rapidly reduced. It resulted from the decrease of proton concentration and the fact that  $H_2$  evolution became more thermodynamically unfavorable with increasing pH values [19,47]. The effect of  $AgI$  loading on the surface of  $g-C_3N_4$  was also carried out to optimize the reaction condition and the results were shown in Fig. 8. The activity of  $H_2$  evolution increased with the  $AgI$  loading increase. When the  $AgI$  loading was 0.1  $\mu\text{mol}$ , the highest activity of  $H_2$  evolution was achieved, corresponding to 104.3  $\mu\text{mol}$  in 3 h. Further increase of the  $AgI$  loading, even though the  $I_3^-$  and  $I_5^-$  increased, the activity of  $H_2$  evolution remained constant. These results might result from the  $Ag$  NPs agglomeration, which led to exposing less active site for HER. In order to prove the  $Ag$  NPs agglomeration, the TEM was carried out and the result was shown in Fig. 9. On the surface of 20 mg  $g-C_3N_4$ , the size of 0.2  $\mu\text{mol}$   $Ag$  NPs was larger than that of 0.1  $\mu\text{mol}$   $Ag$  NPs. By a statistics about 300 NPs, the size of low loading was in the range of 4–16 nm and the maximum distribution of  $Ag$  NPs in 8 nm was about 39.3%. However, the size of high loading was in the range of 8–22 nm and the maximum distribution of  $Ag$  NPs in 16 nm was about 30.4%. In addition, the amount of EY for  $H_2$  evolution was also carried out to optimize the reaction condition and the results were shown in Fig. 10. The highest activity of  $H_2$  evolution was achieved when the amount of EY was 52 mg, corresponding to 104.3  $\mu\text{mol}$  in 3 h.

Photoelectrochemical experiments were performed to study the photoinduced electron transfer processes. As shown in Fig. 11, the response to visible light could be seen during on–off cycles of visible light irradiation, while the  $g-C_3N_4/ITO$  and  $I-g-C_3N_4/ITO$  electrodes produced low photocurrents. The observed unbiased transient photocurrent of  $g-C_3N_4/Ag/ITO$  electrode was promoted under similar experimental conditions. The maximum photocurrent was 11.8  $\mu\text{A}/\text{cm}^2$  after sensitized by EY. This result indicated that the  $Ag$  NPs could enhance the cathodic photocurrent. However, after loading  $I_3^-$  and  $I_5^-$  on the surface of  $g-C_3N_4$ , the photocurrent was further enhanced, the corresponding maximum photocurrent was 18.1  $\mu\text{A}/\text{cm}^2$ . It implied that the  $I_3^-$  and  $I_5^-$  could enhance the electron transfer on the surface of  $g-C_3N_4$  to remarkably reduce the recombination of carrier and prolonged the lifetime of photo-generated charges, which eventually led to excellent  $H_2$  evolution activity [48]. In addition, the electrochemical  $H_2$  evolution activities of photocatalysts deposited on ITO glass were also investigated using the linear sweep voltammetry (LSV) technique. As shown in Fig. 12, the cathodic current of bare ITO electrode belonged to the reduction of water to  $H_2$  was low with the increase of the

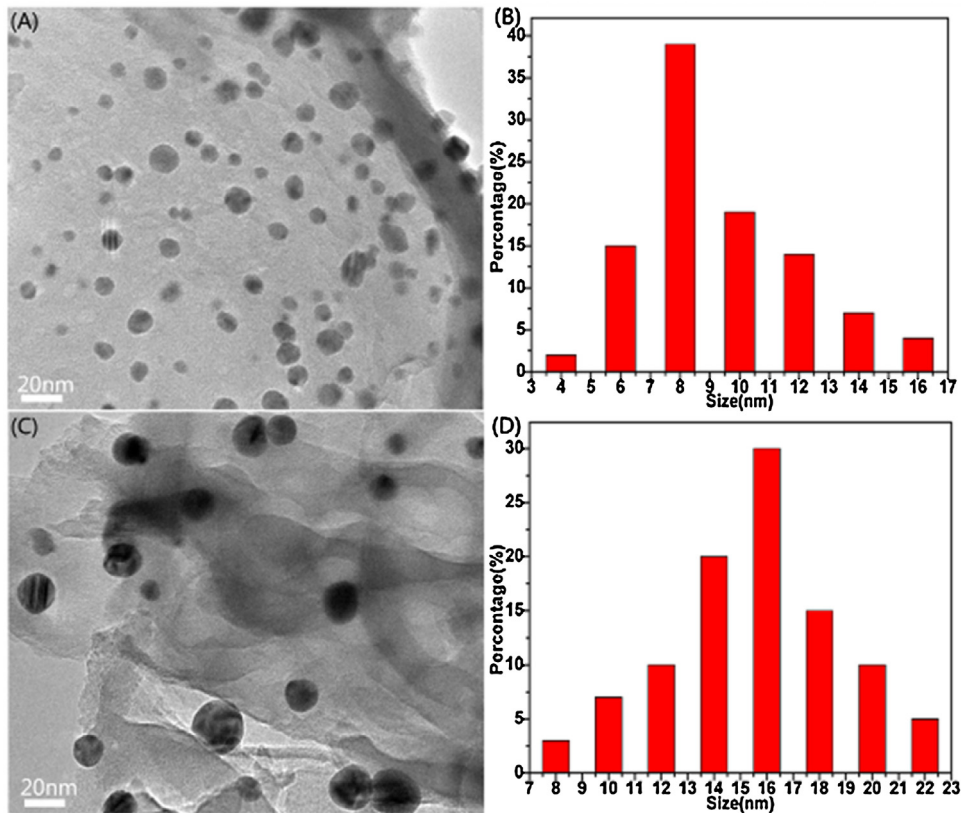


**Fig. 9.** Transmission electron microscopy images of 0.1 (A) and 0.2 (C)  $\mu\text{mol}$  Ag NPs on the surface of  $\text{g-C}_3\text{N}_4$  photocatalyst; the particle size distribution of 0.1 (B) and 0.2 (D)  $\mu\text{mol}$  Ag NPs on the surface of  $\text{g-C}_3\text{N}_4$  photocatalyst.

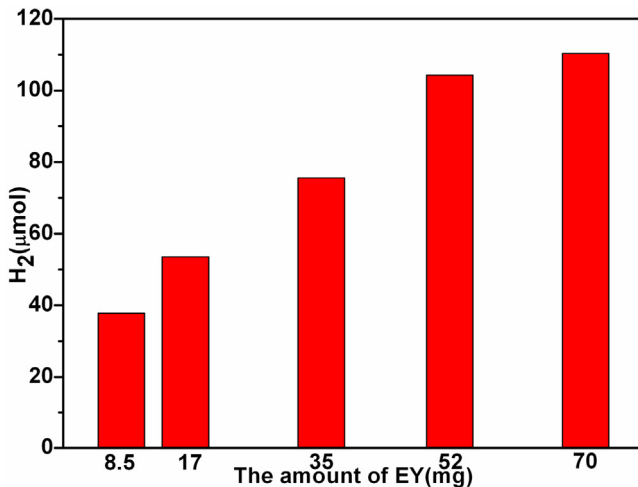


**Fig. 10.** The effect of the EY amount on the activity of  $\text{H}_2$  evolution over I-g- $\text{C}_3\text{N}_4$ /Ag photocatalyst under visible light irradiation.

applied potential [49]. The cathodic currents of  $\text{g-C}_3\text{N}_4$ /ITO and I-g- $\text{C}_3\text{N}_4$ /ITO electrodes only had a relative enhancement. However, the  $\text{g-C}_3\text{N}_4$ /Ag/ITO electrode exhibited a significant improvement at  $-0.6$  V, which proved that Ag NPs were remarkable active sites for catalyzing the water reduction to  $\text{H}_2$  efficiently. Moreover, after the  $\text{I}_3^-$  and  $\text{I}_5^-$  clusters loading on the surface of  $\text{g-C}_3\text{N}_4$ , the photocurrent was further enhanced,  $168 \mu\text{A}/\text{cm}^2$  was achieved at  $-0.6$  V. It further suggested the  $\text{I}_3^-$  and  $\text{I}_5^-$  could enhance the electron transfer on the surface of  $\text{g-C}_3\text{N}_4$  to remarkably reduce the recombination of carrier and prolonged the lifetime of photogenerated

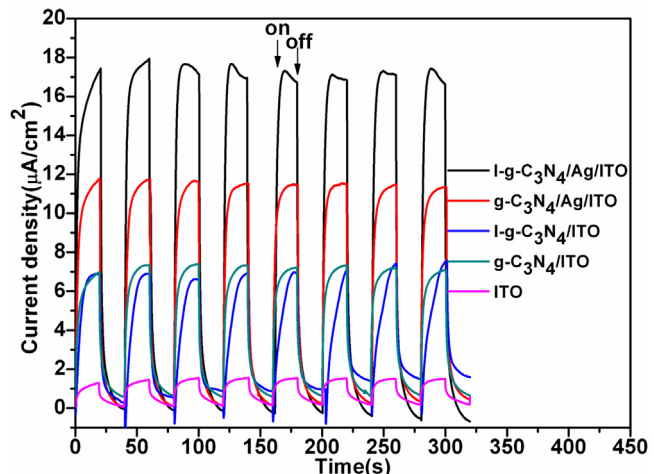


**Fig. 11.** Transient photocurrent time profiles of photocatalysts with EY sensitization on ITO glass in mixed solution of 10% (v/v) TEOA and 0.1 M  $\text{Na}_2\text{SO}_4$  at pH 9 under visible light irradiation ( $\geq 420$  nm).

charges, which eventually led to excellent  $\text{H}_2$  evolution activity (Fig. 13).

The apparent quantum efficiencies (AQEs) were investigated in the range of  $430 \sim 600$  nm using various bandpass filters ( $\lambda = 460, 490, 520, 550$ , and  $590$  nm). Fig. 13 showed that the AQEs value decreased gradually with the incident light wavelength increased, due to the higher potential of photons [50]. However, the highest AQE reached 7.3% at  $520$  nm because of the highest absorption of EY at  $518$  nm. This result indicated that the EY had an interaction with  $\text{g-C}_3\text{N}_4$ , which could lead the electron to transfer faster from excited EY to  $\text{g-C}_3\text{N}_4$ . The stabilities of  $\text{H}_2$  evolution over I-g-

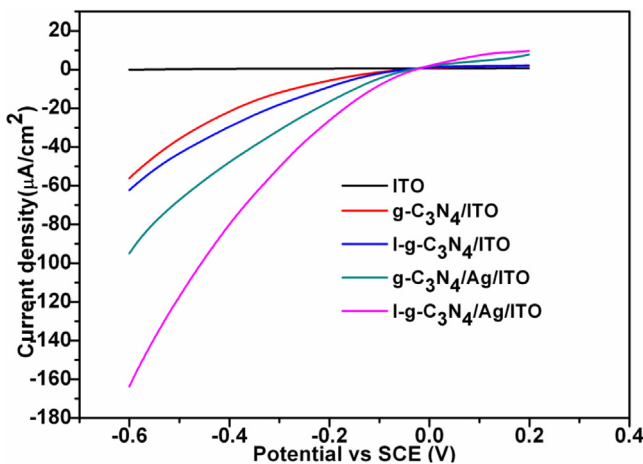


**Fig. 12.** LSV curves of photocatalysts coated on ITO glass in mixed solution of 10% (v/v) TEOA and 0.1 M  $\text{Na}_2\text{SO}_4$  aqueous solution.

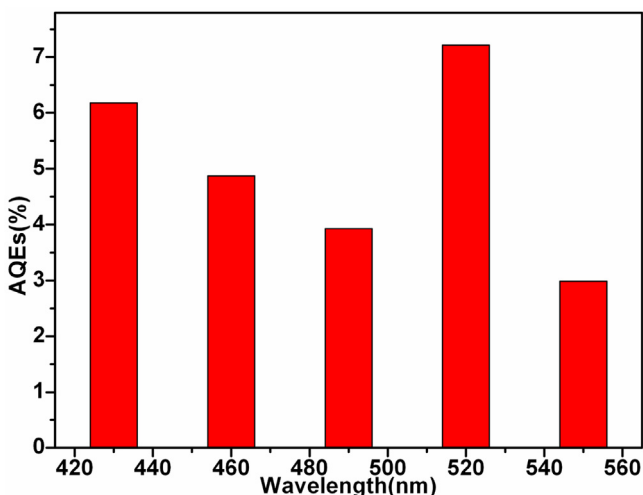


**Fig. 13.** The apparent quantum efficiencies (AQEs) of I-g-C<sub>3</sub>N<sub>4</sub>/Ag photocatalyst with EY sensitization under a wide range of visible light irradiation from 400 to 600 nm.

$\text{C}_3\text{N}_4/\text{Ag}$  photocatalyst sensitized by EY were tested under visible light irradiation ( $\lambda \geq 420$  nm). As shown in **Fig. 14**, the catalysts were stable during 900 min reaction. After each run, the catalysts were collected by centrifuging from the reaction mixture and redistributed in the fresh TEOA aqueous solution. The rates of  $\text{H}_2$  evolution remained almost no change in every run. These results indicated that the I-g-C<sub>3</sub>N<sub>4</sub>/Ag catalyst was significantly stable during the photocatalytic  $\text{H}_2$  evolution processes.

The theoretical model of the tunneling of an electron between two carbon atoms of g-C<sub>3</sub>N<sub>4</sub> through the polyiodides p orbitals opened additional channels for hopping in I-g-C<sub>3</sub>N<sub>4</sub> has been built as shown in **Scheme 2**. For the  $\text{I}_3^-$  and  $\text{I}_5^-$  clusters, the linear chain structures were more stability due to they have a lower ground-state energy [35]. The distances of  $\text{I}_3^-$  and  $\text{I}_5^-$  clusters were about 5.80 and 12.04 Å, respectively [51]. In addition, the radius of I atom was about 1.95 Å, which indicated the maximum distances of an electron hopping through  $\text{I}_3^-$  and  $\text{I}_5^-$  clusters were about 9.7 and 15.94 Å, respectively. As the **Scheme 2** shown, the C–N bond length of g-C<sub>3</sub>N<sub>4</sub> was about 1.32 Å [52], the results of geometric calculation showed the distance of C1–C2, C1–C3, C4–C5 and C4–C6 corresponded to 8.24, 10.48, 14.99 and 16.49 Å. This result implied, in geometry, the  $\text{I}_3^-$  and  $\text{I}_5^-$  clusters could spin-orbit coupling with C1–C2 and C4–C5 by living active electrons in p orbitals, which led to

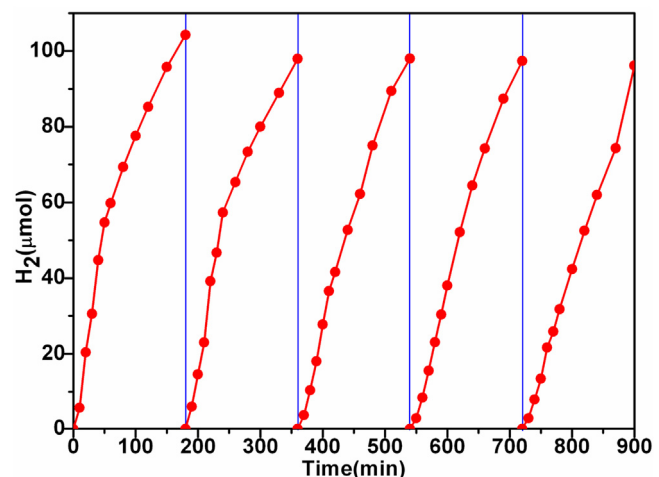
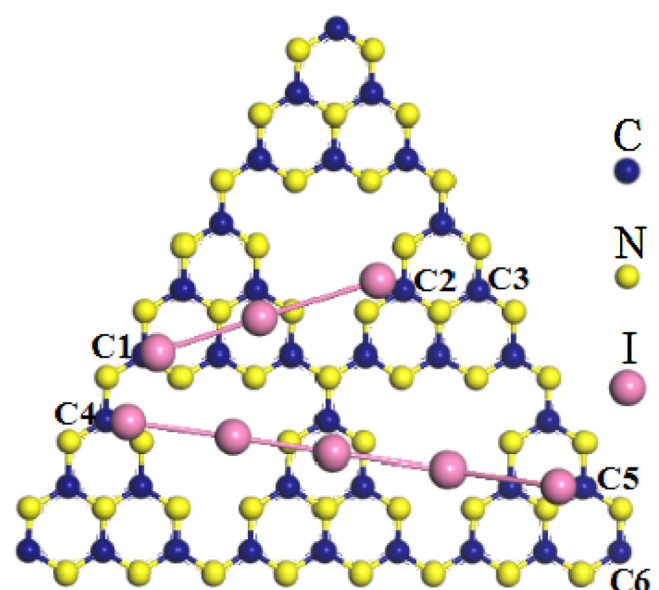


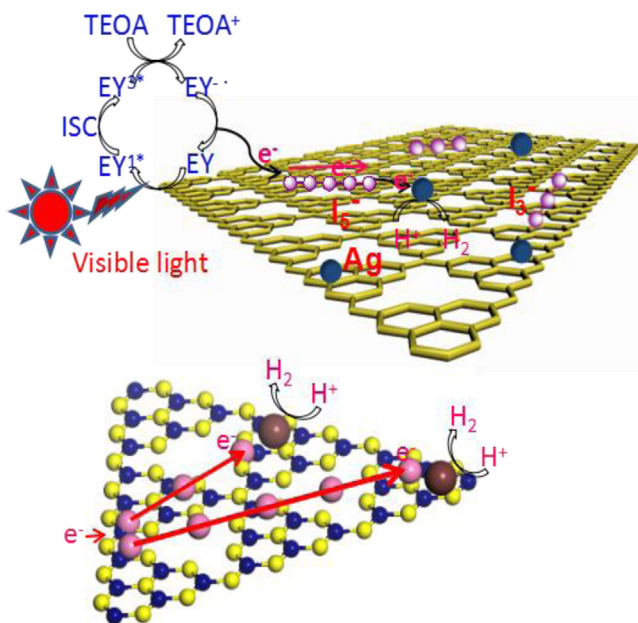
**Fig. 14.** The stabilities of  $\text{H}_2$  evolution over I-g-C<sub>3</sub>N<sub>4</sub>/Ag photocatalyst under visible light irradiation ( $\lambda \geq 420$  nm). After every run, the catalysts were collected by centrifuging from the reaction mixture and redistributed in the fresh 10% TEOA aqueous solution.

an electron could hop from C1 to C2 through the additional channel opened by  $\text{I}_3^-$  clusters and from C4 to C5 through the another additional channel opened by  $\text{I}_5^-$  clusters. It was also key point for the excellent conductivity of I-g-C<sub>3</sub>N<sub>4</sub> and high  $\text{H}_2$  evolution activity over I-g-C<sub>3</sub>N<sub>4</sub>/Ag photocatalyst.

The reaction process of photocatalysis  $\text{H}_2$  evolution over the sensitized I-g-C<sub>3</sub>N<sub>4</sub>/Ag photocatalyst can be explained in terms of **Scheme 3**. The EY molecule absorbed visible light photon to form singlet excited state  $\text{EY}^{1*}$  under visible light irradiation, and then produced the lowest-lying triplet excited state  $\text{EY}^{3*}$  via an efficient intersystem crossing.  $\text{EY}^{3*}$  can be reductively quenched by TEOA and produce  $\text{EY}^{\cdot-}$  and oxidative donor ( $\text{TEOA}^+$ ) [53]. The  $\text{e}^-$  of  $\text{EY}^{\cdot-}$  specie was transferred to g-C<sub>3</sub>N<sub>4</sub> by the noncovalent  $\pi$ - $\pi$  stacking interaction due to its electron transport characteristics, which led to spatial separation of photogenerated charges [8]. The accumulated electrons on the surface of g-C<sub>3</sub>N<sub>4</sub> would transfer to active site Ag NPs along the  $\text{I}_3^-$  and  $\text{I}_5^-$  in a straight line rather than along folded chemical bond of g-C<sub>3</sub>N<sub>4</sub> since the tunneling of an



**Scheme 2.** The model of electrons hopped distance through the additional channels of the  $\text{I}_3^-$  and  $\text{I}_5^-$  clusters.



**Scheme 3.** The proposed reaction mechanism for visible-light-driven water splitting by I-g-C<sub>3</sub>N<sub>4</sub>/Ag photocatalyst with EY sensitization.

electron between two far-located carbon atoms of g-C<sub>3</sub>N<sub>4</sub> through the polyiodides p orbitals opened additional channels for electron hopping in I-g-C<sub>3</sub>N<sub>4</sub>, which gave rise to the superior charge transfer performance to remarkably reduce the recombination of carrier and prolonged the lifetime of photogenerated charges.

#### 4. Conclusion

In this work, the I<sub>3</sub><sup>−</sup> and I<sub>5</sub><sup>−</sup> decorated g-C<sub>3</sub>N<sub>4</sub> was prepared for hydrogen evolution by in situ AgI NPs decomposition driven by visible light irradiation. The significant electron tunneling over iodine-decorated graphitic carbon nitride (I-g-C<sub>3</sub>N<sub>4</sub>) was achieved by I<sub>3</sub><sup>−</sup> and I<sub>5</sub><sup>−</sup> cluster implanted. The flip-flop electron tunneling takes place via strong Rashba spin-orbit coupling in p orbitals of polyiodides. The electron tunneling and hopping bridged the easier transfer route between far-located carbon atoms of g-C<sub>3</sub>N<sub>4</sub> through the polyiodides p orbitals for enhancing the H<sub>2</sub> evolution over Ag active site. By taking the advantage of this tunneling, the I-V characteristics and PL spectra showed the conductivity of I-g-C<sub>3</sub>N<sub>4</sub>/Ag photocatalyst was remarkably increased and the lifetime of photogenerated charges was largely prolonged. With the help of these properties, the obtained I-g-C<sub>3</sub>N<sub>4</sub>/Ag photocatalyst present a highly active for hydrogen generation under visible light irradiation. About 104.3 μmol H<sub>2</sub> was evolved over I-g-C<sub>3</sub>N<sub>4</sub>/Ag photocatalyst in 3 h, about three time higher than that of un-iodinated g-C<sub>3</sub>N<sub>4</sub>/Ag, and no remarkable decay of activity was observed in 900 min reaction. The highest AQE value of 7.3% was achieved at 520 nm.

#### Acknowledgment

This work is supported by the NSF of China (grant nos. 21433007 and 21673262), respectively.

#### References

- R.S. Sprick, B. Bonillo, R. Clowes, P. Guiglion, N.J. Brownbill, B.J. Slater, F. Blanc, M.A. Zwijnenburg, D.J. Adams, A.I. Cooper, *Angew. Chem. Int. Ed.* 55 (2016) 1792–1796.
- L. Ma, X. Kang, S. Hu, F. Wang, *J. Mol. Catal. (China)* 29 (2015) 359–368.
- Z. Li, B. Tian, W.L. Zhen, Y.Q. Wu, G.X. Lu, *Appl. Catal. B* 203 (2017) 408–415.
- S. Ghosh, N.A. Kouamé, L. Ramos, S. Remita, A. Dazzi, A. Deniset-Besseau, P. Beaunier, F. Goubard, P. Aubert, H. Remita, *Nat. Mater.* 14 (2015) 505–511.
- S. Peng, M. Ding, T. Yi, Y. Li, *J. Mol. Catal. (China)* 28 (2014) 466–473.
- K. Kailasam, M.B. Mesch, L. Möhlmann, M. Baar, S. Blechert, M. Schwarze, M. Schröder, R. Schomäcker, J. Senker, A. Thomas, *Energy Technol.* 4 (2016) 744–750.
- K. Maeda, K. Teramura, N. Saito, Y. Inoue, K. Domen, *J. Catal.* 243 (2006) 303–308.
- S.X. Min, G.X. Lu, *J. Phys. Chem. C* 116 (2012) 25415–25424.
- S.X. Min, G.X. Lu, *J. Phys. Chem. C* 116 (2012) 19644–19652.
- Z. Li, C. Kong, G.X. Lu, *Int. J. Hydrogen Energy* 40 (2015) 9061–9068.
- H.D. Li, L. Wang, Z.H. Lan, Y.S. Zheng, *Phys. Rev. B* 79 (2009) 155429.
- K.S. Novoselov, A.K. Geim, S.V. Morozov, D. Jiang, Y. Zhang, S.V. Dubonos, I.V. Grigorieva, A.A. Firsov, *Science* 306 (2004) 666–669.
- A.K. Geim, K.S. Novoselov, *Nat. Mater.* 6 (2007) 183–191.
- M.J. Allen, V.C. Tung, R.B. Kaner, *Chem. Rev.* 110 (2010) 132–135.
- H. Zhang, X.J. Lv, Y.M. Li, Y. Wang, J.H. Li, *ACS Nano* 4 (2010) 380–386.
- C. Chen, W.M. Cai, M.C. Long, B.X. Zhou, Y.H. Wu, D.Y. Wu, Y.J. Feng, *ACS Nano* 4 (2010) 6425–6432.
- G.G. Zhang, Z.A. Lan, X.C. Wang, *Angew. Chem. Int. Ed.*, 10.1002/anie.201607375.
- Y.J. Wang, R. Shi, J. Lin, Y.F. Zhu, *Energy Environ. Sci.* 4 (2011) 2922–2929.
- Z. Li, Q.S. Wang, C. Kong, Y.Q. Wu, Y.X. Li, G.X. Lu, *J. Phys. Chem. C* 119 (2015) 13561–13568.
- X.Y. Zhang, H.P. Li, X.L. Cui, Y.H. Lin, *J. Mater. Chem.* 20 (2010) 2801–2806.
- Y.H. Ng, A. Iwase, A. Kudo, R. Amal, *J. Phys. Chem. Lett.* 1 (2010) 2607–2612.
- G. Eda, G. Fanchini, M. Chhowalla, *Nat. Nanotechnol.* 3 (2008) 270–274.
- H.L. Wang, J.T. Robinson, X.L. Li, H.J. Dai, *J. Am. Chem. Soc.* 131 (2009) 9910–9911.
- D. Wang, S. Hasegawa, M. Shimizu, J. Tanaka, *Synth. Met.* 46 (1992) 85–91.
- X.R. Zeng, T.M. Ko, *J. Polym. Sci. B: Polym. Phys.* 35 (1997) 1993–2001.
- Z. Yao, H.G. Nie, Z. Yang, X.M. Zhou, Z. Liu, S.M. Huang, *Chem. Commun.* 48 (2012) 1027–1029.
- W.Y. Zhou, S.S. Xie, L.F. Sun, D.S. Tang, Y.B. Li, Z.Q. Liu, L.J. Ci, X.P. Zou, G. Wang, *Appl. Phys. Lett.* 80 (2002) 2553–2555.
- I.Y. Jeon, H.J. Choi, M. Choi, J.M. Seo, S.M. Jung, M.J. Kim, S. Zhang, L.P. Zhang, Z.H. Xia, L.M. Dai, N. Park, J.B. Baek, *Sci. Rep.* 3 (2013) 1810.
- N. Jung, N. Kim, S. Jockusch, N.J. Turro, P. Kim, L. Brus, *Nano Lett.* 9 (2009) 4133–4137.
- G. Kalita, K. Wakita, M. Takahashib, M. Umeno, *J. Mater. Chem.* 21 (2011) 15209–15213.
- Y.F. Zhan, B.D. Zhang, L.M. Cao, X.X. Wu, Z.P. Lin, X. Yu, X.X. Zhang, D.R. Zeng, F.Y. Xie, W.H. Zhang, J. Chen, H. Meng, *Carbon* 94 (2015) 1–8.
- L. Grigorian, K.A. Williams, S. Fang, G.U. Sumanasekera, A.L. Loper, E.C. Dickey, S.J. Pennycook, P.C. Eklund, *Phys. Rev. Lett.* 80 (1998) 5560–5563.
- T. Michel, L. Alvarez, J.L. Sauvajol, R. Almairac, R. Aznar, O. Mathon, J.L. Bantignies, E. Flahaut, *J. Phys. Chem. Solids* 67 (2006) 1190–1192.
- G.G. Zhang, M.W. Zhang, X.X. Ye, X.Q. Qiu, S. Lin, X.C. Wang, *Adv. Mater.* 26 (2014) 805–809.
- X.Q. Zhang, G.X. Lu, *Carbon* 108 (2016) 215–224.
- X.C. Wang, K. Maeda, X.F. Chen, K. Takanabe, K. Domen, Y.D. Hou, X.Z. Fu, M. Antonietti, *J. Am. Chem. Soc.* 131 (2009) 1680–1681.
- X.F. Chen, Y.S. Jun, K. Takanabe, K. Maeda, K. Domen, X.Z. Fu, M. Antonietti, X.C. Wang, *Chem. Mater.* 21 (2009) 4093–4095.
- X.C. Wang, K. Maeda, A. Thomas, K. Takanabe, G. Xin, J.M. Carlsson, K. Domen, M. Antonietti, *Nat. Mater.* 8 (2009) 76–80.
- Z. Li, C. Kong, G.X. Lu, *J. Phys. Chem. C* 120 (2016) 56–63.
- T. Komatsu, T. Nakamura, *J. Mater. Chem.* 11 (2001) 474–478.
- V.N. Khabashesku, J.L. Zimmerman, J.L. Margrave, *Chem. Mater.* 12 (2000) 3264–3270.
- Q.X. Guo, Y. Xie, X.J. Wang, S.Y. Zhang, T. Hou, S.H. Lv, *Chem. Commun.* 1 (2004) 26–27.
- A. Thomas, A. Fischer, F. Goettmann, M. Antonietti, J.O. Müller, R. Schlögl, J.M. Carlsson, *J. Mater. Chem.* 18 (2008) 4893–4908.
- T. Shimizu, T. Iyoda, Y. Koide, *J. Am. Chem. Soc.* 107 (1985) 35–41.
- Q.Y. Li, L. Chen, G.X. Lu, *J. Phys. Chem. C* 111 (2007) 11494–11499.
- Z. Li, Y.Q. Wu, G.X. Lu, *Appl. Catal. B* 188 (2016) 56–64.
- K. Kalyanasundaram, J. Kiwi, M. Graetzel, *Helv. Chim. Acta* 61 (1978) 2720–2730.
- A. Wojcik, P.V. Kamat, *ACS Nano* 4 (2010) 6697–6706.
- X. Zong, G.P. Wu, H.J. Yan, G.J. Ma, J.Y. Shi, F.Y. Wen, L. Wang, C. Li, *J. Phys. Chem. C* 114 (2010) 1963–1968.
- H.J. Yan, J.H. Yang, G.J. Ma, G.P. Wu, X. Zong, Z.B. Lei, J.Y. Shi, C. Li, *J. Catal.* 266 (2009) 165–168.
- A.A. Tonkikh, E.D. Obraztsova, E.A. Obraztsova, A.V. Belkin, A.S. Pozharov, *Phys. Status Solidi B* 249 (2012) 2454–2459.
- P. Kroll, R. Hoffmann, *J. Am. Chem. Soc.* 121 (1999) 4696–4703.
- K. Maeda, M. Eguchi, S.H.A. Lee, W.J. Youngblood, H. Hata, T.E. Mallouk, *J. Phys. Chem. C* 113 (2009) 7962–7969.